CU/NCEI IGRF-13 Evaluation

Patrick Alken, Arnaud Chulliat, Manoj Nair, Sam Califf, Neesha Schnepf

November 2019

Contents

1 Introduction

This document contains the University of Colorado at Boulder and National Centers of Environmental Information (NCEI) evaluation of the IGRF-13 candidate models. In what follows, we assign letter codes to each institution which submitted a candidate model, as given in Table 1.

Letter Code	Lead Institution	Team Leader
A	British Geological Survey	W. Brown
B	Institute of Crustal Dynamics, CEA	Y. Yang
C	University of Colorado, Boulder	P. Alken
D	Danish Technical University	C. Finlay
E	GFZ Potsdam	M. Rother
F	Institut de Physique du Globe de Paris	G. Hulot
G	ISTerre	L. Huder
H	Pushkov Institute of Terrestrial Magnetism	V. Petrov
I	Kyoto University	H. Toh
J	Leeds University	P. Livermore
K	Max Planck Institute	S. Sanchez
L	NASA GSFC	T. Sabaka
M	University of Potsdam	J. Baerenzung
N	Universidad Complutense Madrid	F. Javier Pavon Carrasco
O	University of Strasbourg	I. Wardinski

Table 1: IGRF-13 institutions and letter codes

2 Mean and Median Models

We computed the mean and median of all candidate models for each product (DGRF2015, IGRF2020, and IGRF SV2020-2025) in order to compare individual candidates.

3 Spectral Analysis of Candidate Models

In this section we plot the Lowes-Mauersberger spectrum of each candidate, as well as spectral differences with respect to the mean and median models.

3.1 DGRF-2015

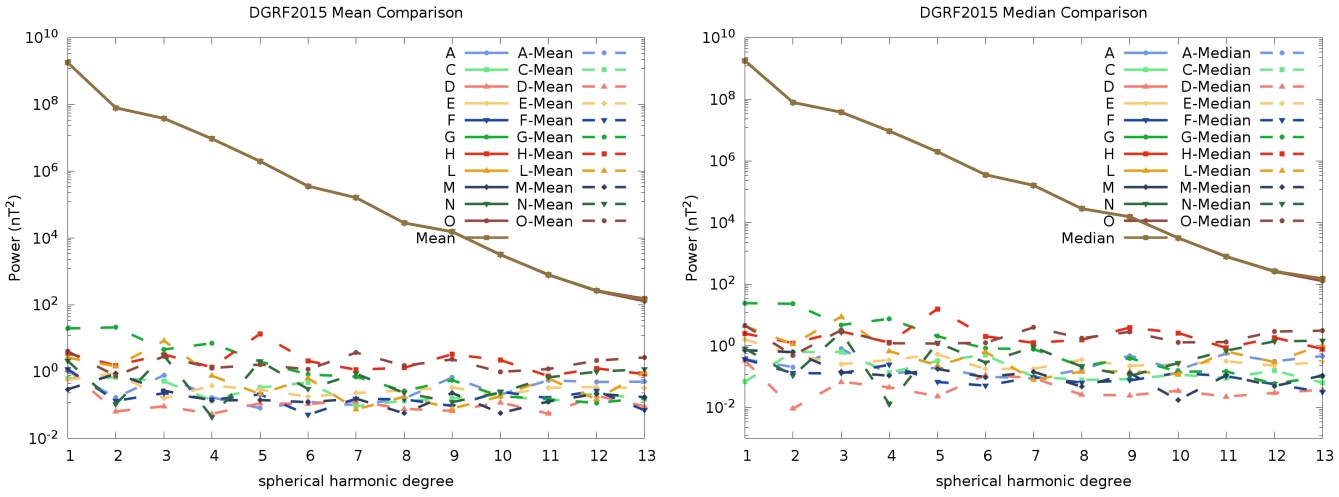

While some models are closer to the mean/median than others, we find no significant outlier model according to the spectral plot.

3.2 IGRF-MF-2020

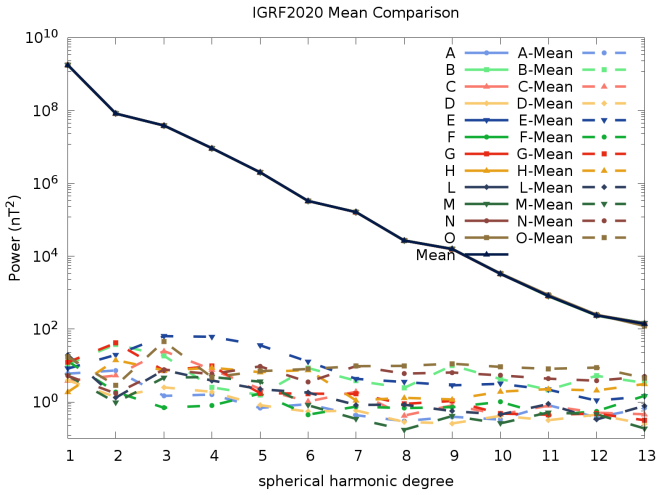

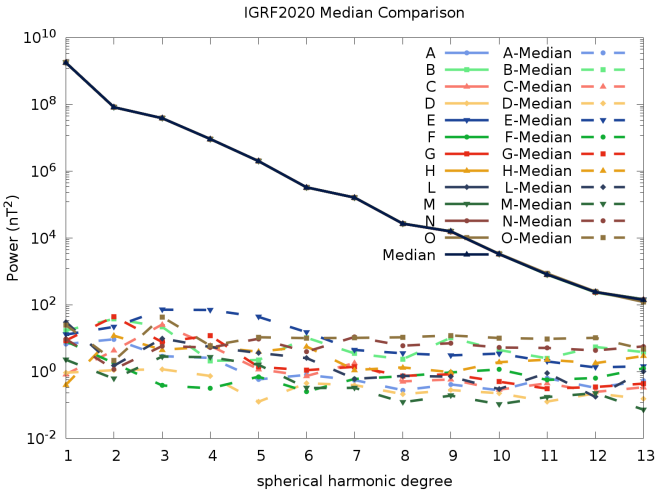

Among the IGRF MF2020 candidates, there is again no obvious outlier model according to the spectral plots.

3.3 IGRF-SV-2020

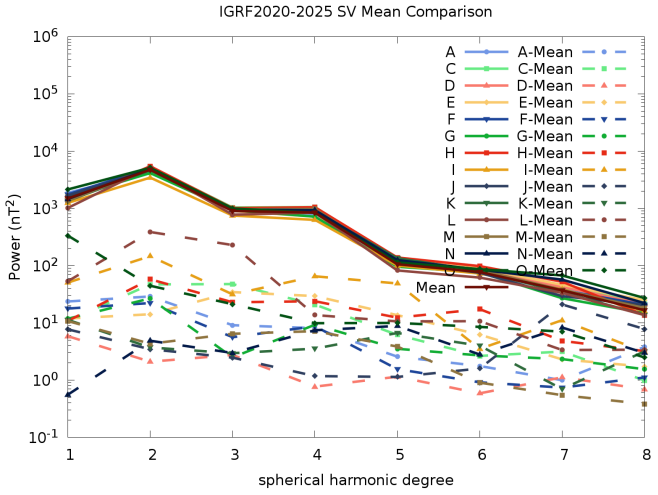

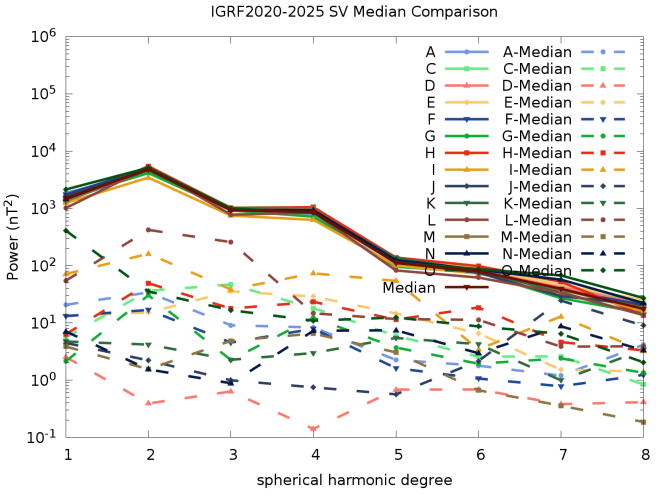

4 Degree Correlations of Candidate Models

4.1 DGRF-2015

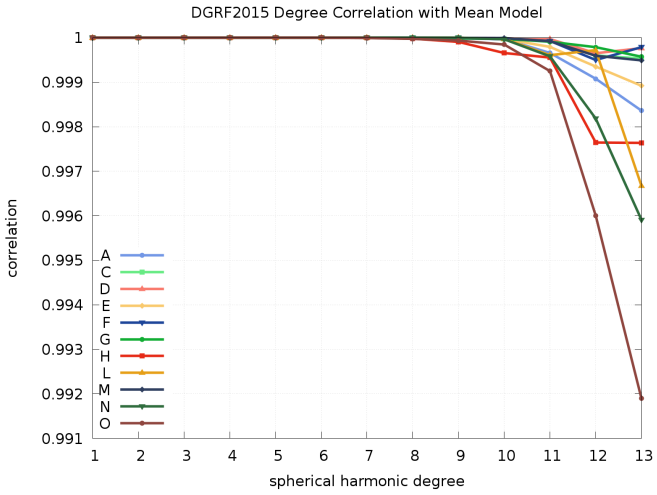

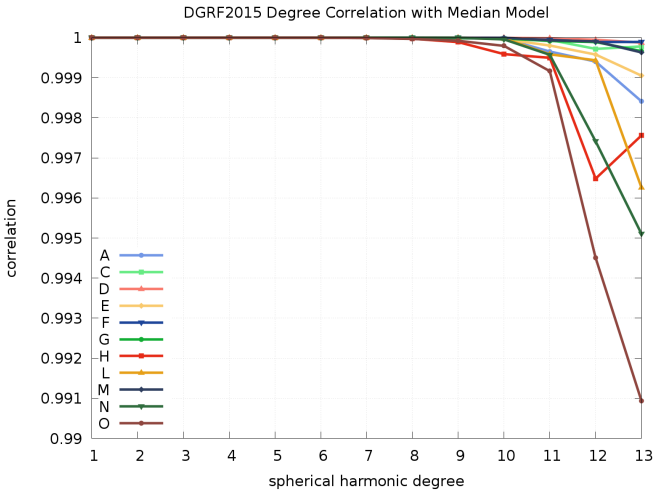

4.2 IGRF-MF-2020

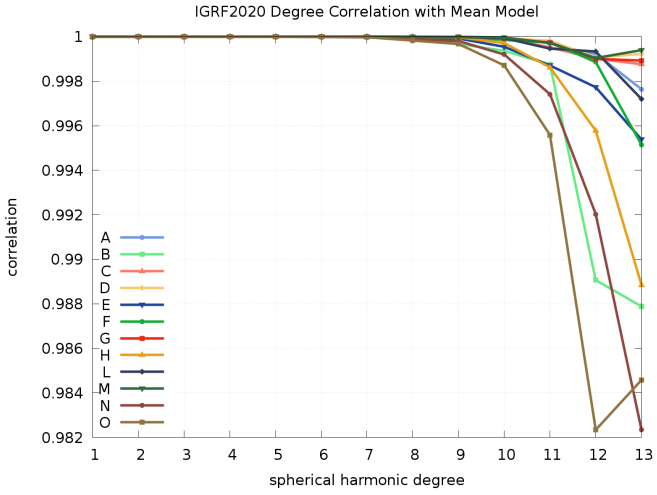

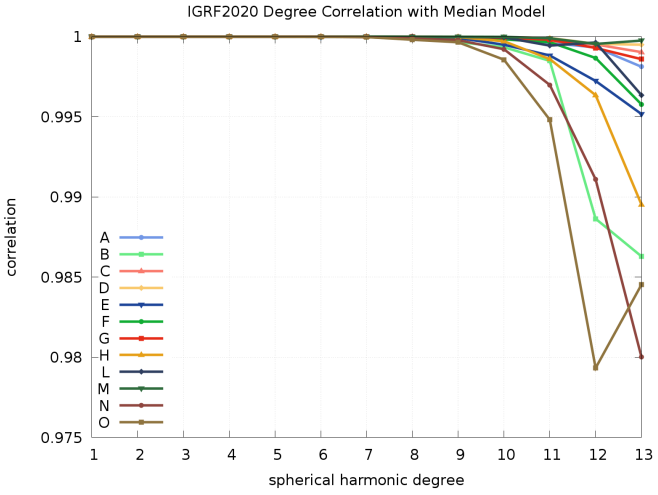

4.3 IGRF-SV-2020

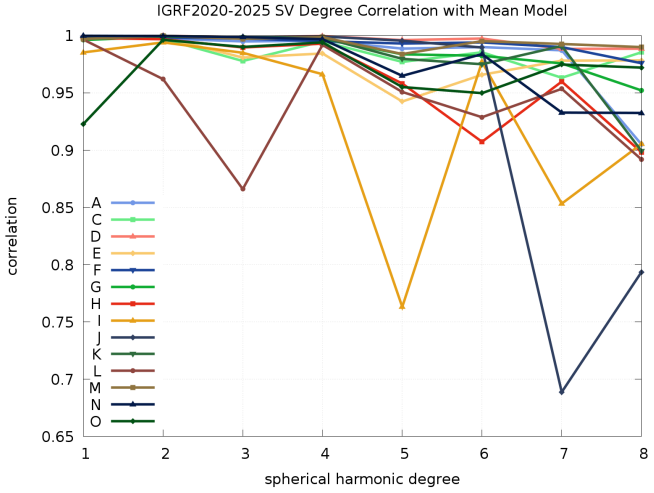

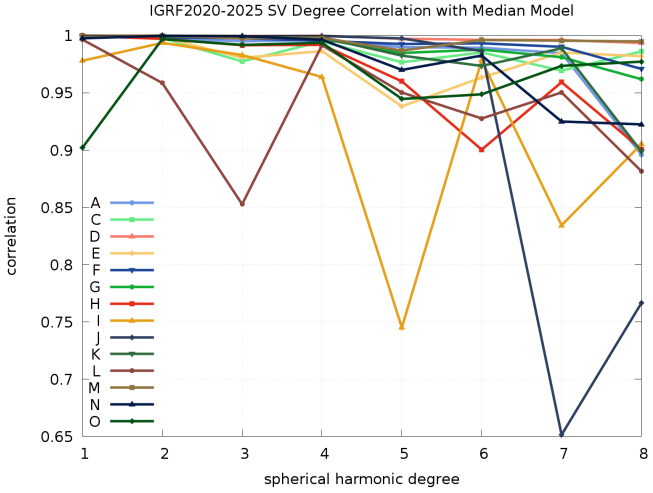

5 Spatial Comparisons of Candidate Models

5.1 DGRF-2015

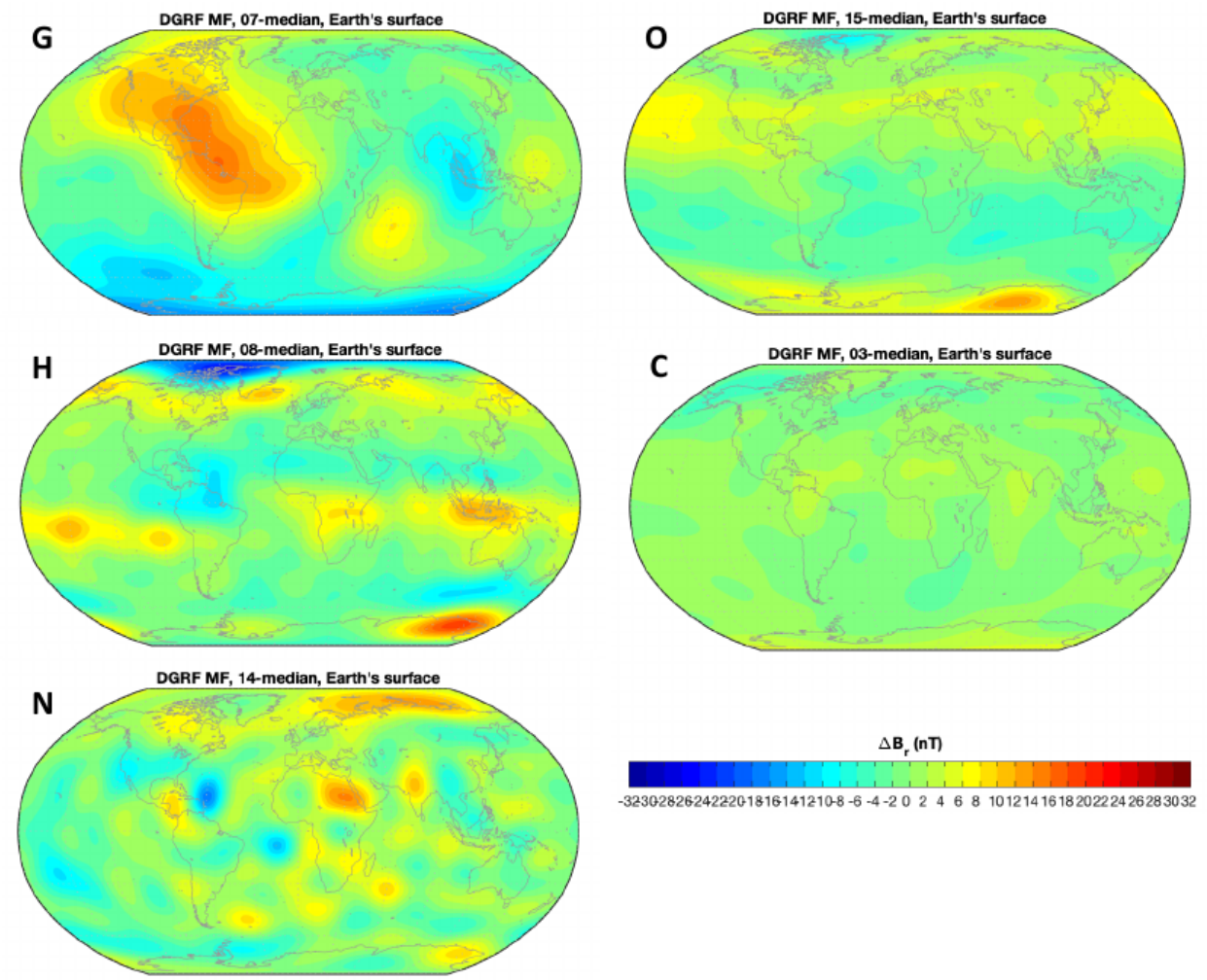

Here we plot spatial maps of differences in the B_r component between various DGRF2015 candidates and the median model, at Earth's surface. Model G shows differences up to 31 nT, localized in the South Atlantic region, while H and N show smaller differences around the globe.

5.2 IGRF-MF-2020

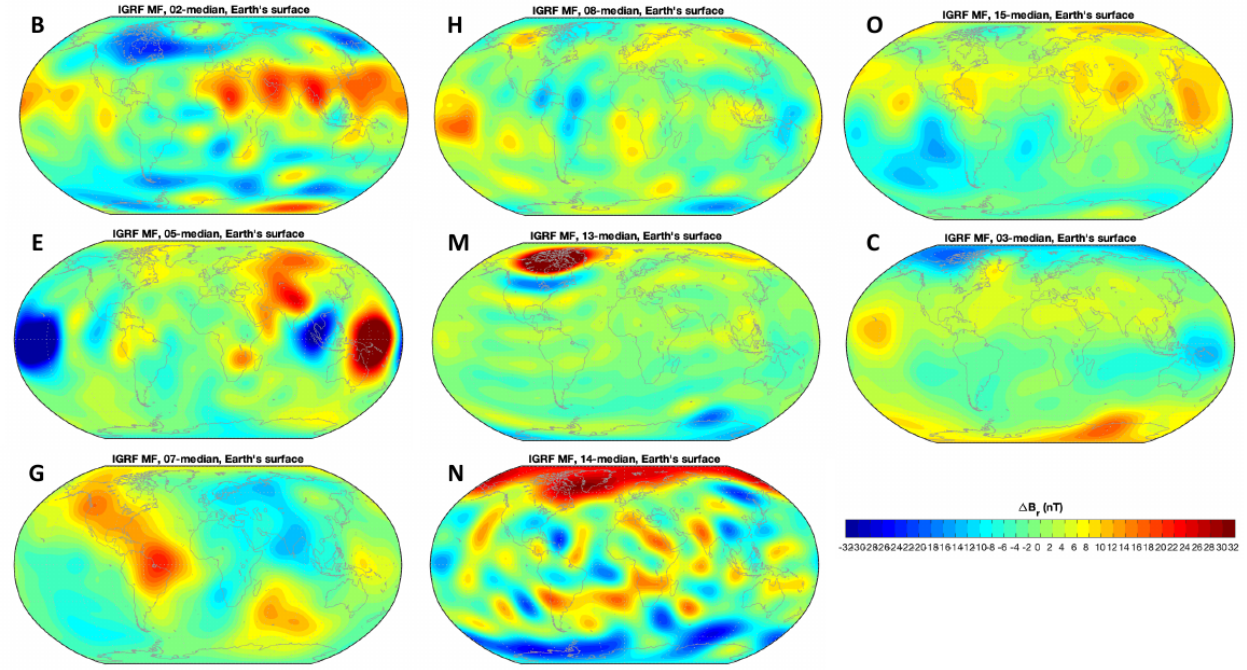

Here we plot spatial maps of the differences of the radial field component B_r between several IGRF2020 main field candidates and the median model at Earth's surface. Several candidates show significant differences up to 93 nT with respect to the median model.

5.3 IGRF-SV-2020

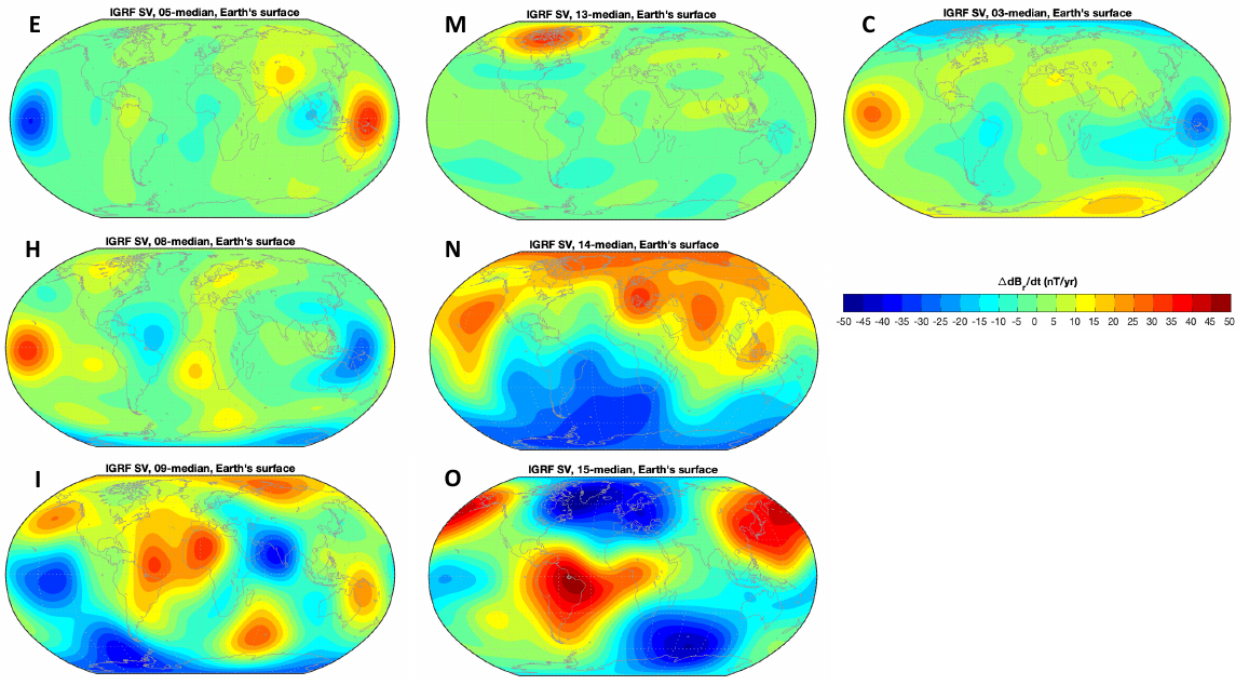

Here we show spatial maps of differences in dB_r/dt of some IGRF2020-2025 SV candidate models with the median model at Earth's surface. Several candidates show differences up to 73 nT/year in various places around the globe. The spatial differences are quite different between the different candidates.

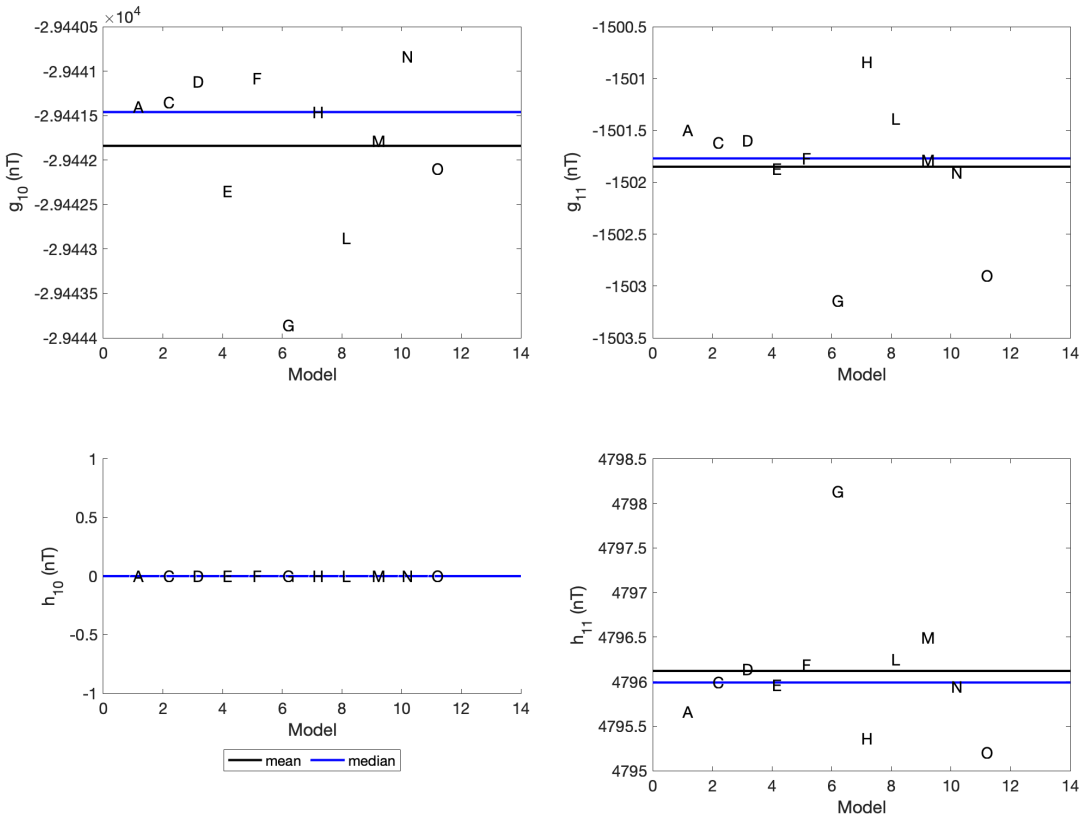

Figure 1: Comparison of the dipole coefficients for each model with the mean (black line) and median (blue line) values.

6 Spherical Harmonic Coefficient Comparisons of Candidate Models

To compare the models, a sensitivity matrix $S(n,m)$ was produced between each model i and the reference mean or median model r. The sensitivity matrices were determined following (Thebault, 2015):

$$S(n,m) = \begin{cases} 100\frac{{}_ig_n^m - {}_rg_n^m}{\sqrt{\frac{1}{2n+1}\sum_{m=0}^{n}({}_rg_n^m)^2+({}_rh_n^m)^2}} & \text{for } m \geq 0, \\ 100\frac{{}_ih_n^m - {}_rh_n^m}{\sqrt{\frac{1}{2n+1}\sum_{m=0}^{n}({}_rg_n^m)^2+({}_rh_n^m)^2}} & \text{for } m < 0. \end{cases} \quad (1)$$

This method uses the Lowes-Mauerberger geomagnetic power spectrum to normalize the difference between the two models so that the sensitivity is expressed in percent for each degree n and order m.

6.1 DGRF-2015

We compared the dipole coefficients for each model and found that most are near one another, however, model G's coefficients consistently were outlying from the rest of the coefficients.

The sensitivity matrices between the DGRF 2015 main field and the mean/median models shows good agreement for the lower degrees, with differences increased in the higher degrees. Figures 2-3 shows both the three models with the smallest average sensitivity percentage and the three models with the largest average sensitivity percentage compared to the mean and median models.

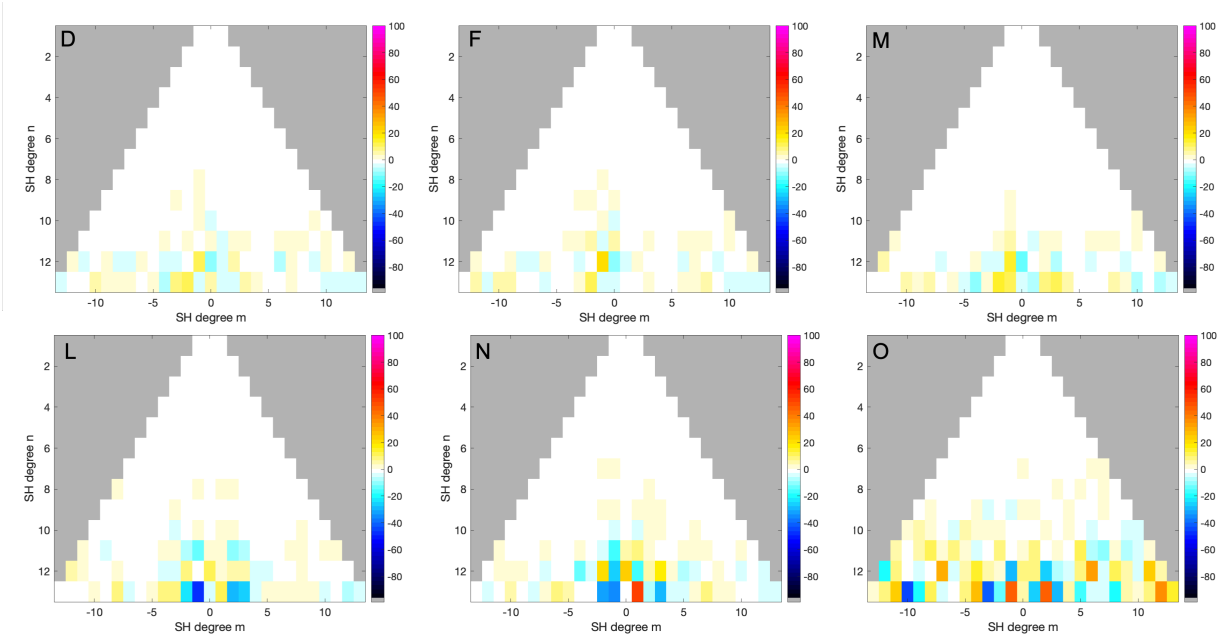

Figure 2: Select sensitivity matrices between a given model (shown here are D, F, M, L, N and O) and the mean DGRF main field model.

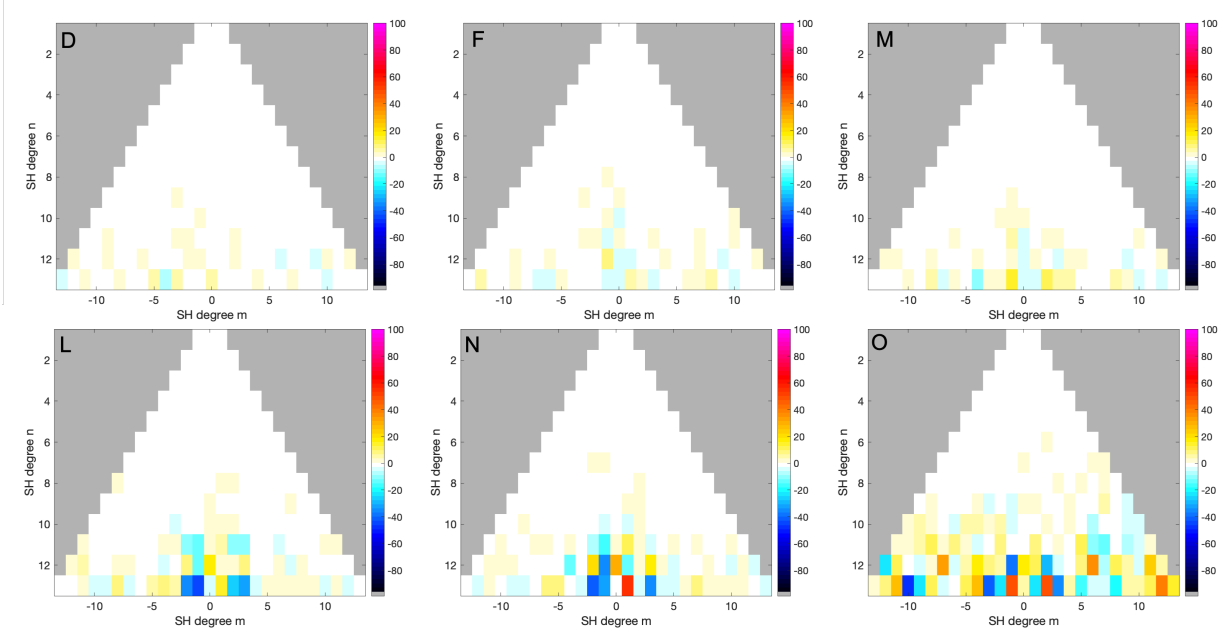

Figure 3: Select sensitivity matrices between a given model (shown here are D, F, M, L, N and O) and the median DGRF main field model.

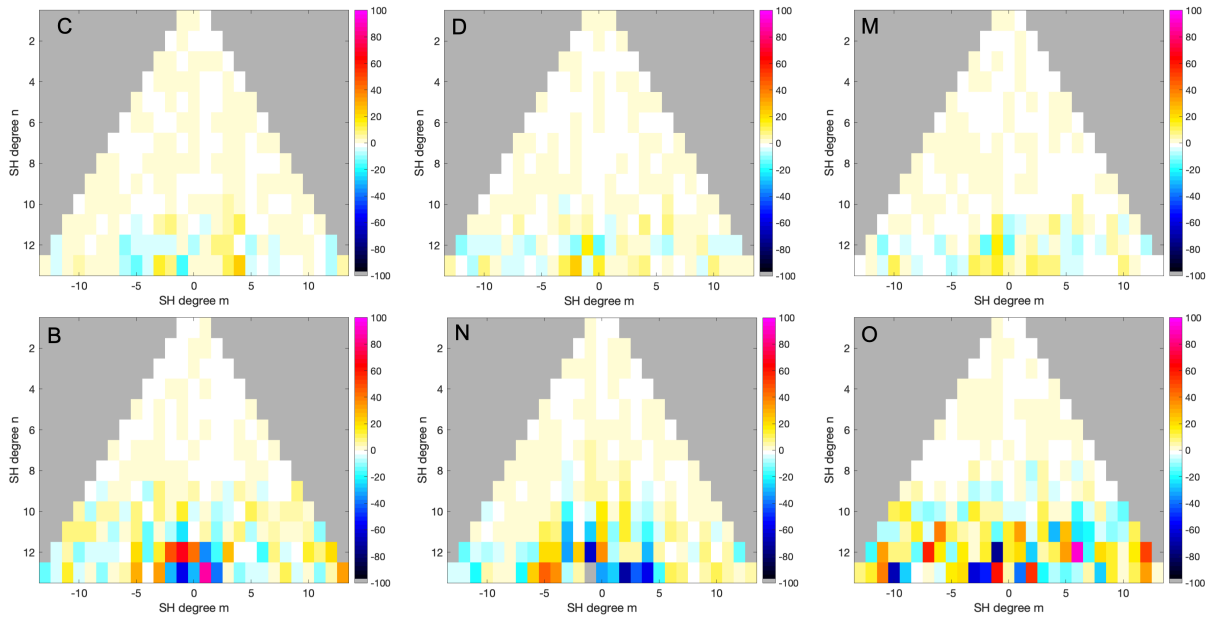

Figure 4: Select sensitivity matrices between a given model (shown here are C, D, M, B, N and O) and the mean IGRF main field model.

6.2 IGRF-MF-2020

We compared the dipole coefficients for each model and found that most are near one another.

The sensitivity matrices between the IGRF 2020 main field and the mean/median models again shows good agreement for the lower degrees, with differences increased in the higher degrees. Figures 4-5 shows both the three models with the smallest average sensitivity percentage and the three models with the largest average sensitivity percentage compared to the mean and median models.

6.3 IGRF-SV-2020

We compared the dipole coefficients for each model and found that most are near one another, with I, O, and L often outlying from the rest.

The sensitivity matrices between the IGRF 2020 secular variation shows a lot of variability. Figure 6 shows the D model's sensitivity matrix compared to the mean (left) and median (right) models. This model was one of the models with the lowest percentage differences. Across all the models, the average sensitivity matrix percentage ranged from 0.6% to 17% difference.

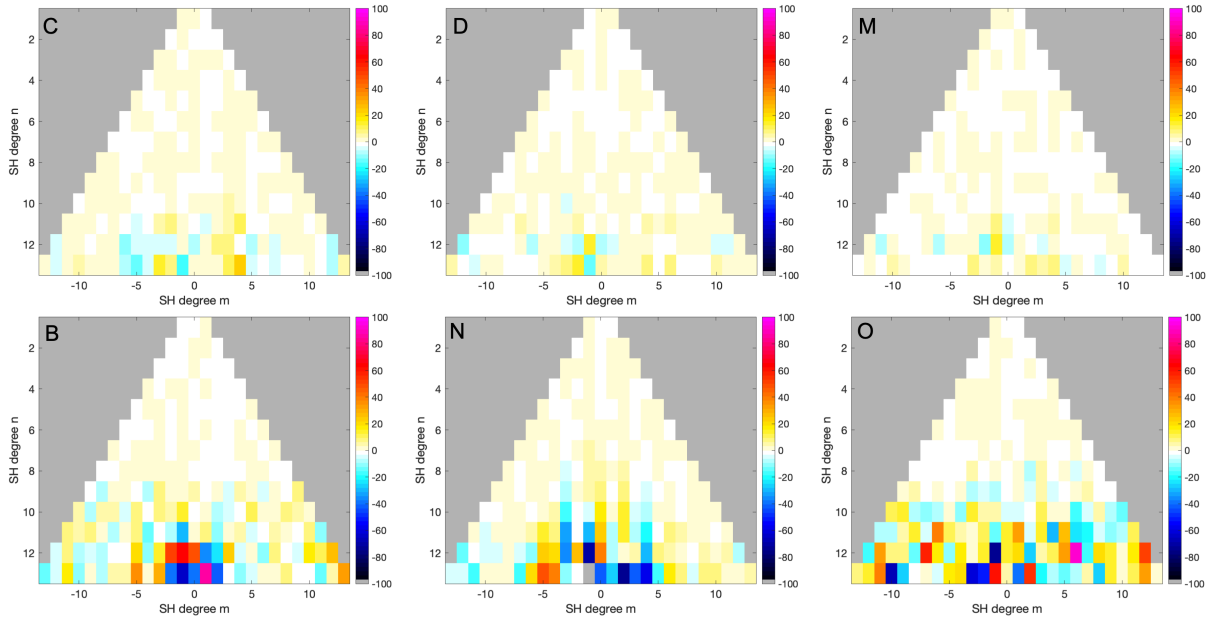

Figure 5: Select sensitivity matrices between a given model (shown here are C, D, M, B, N and O) and the median IGRF main field model.

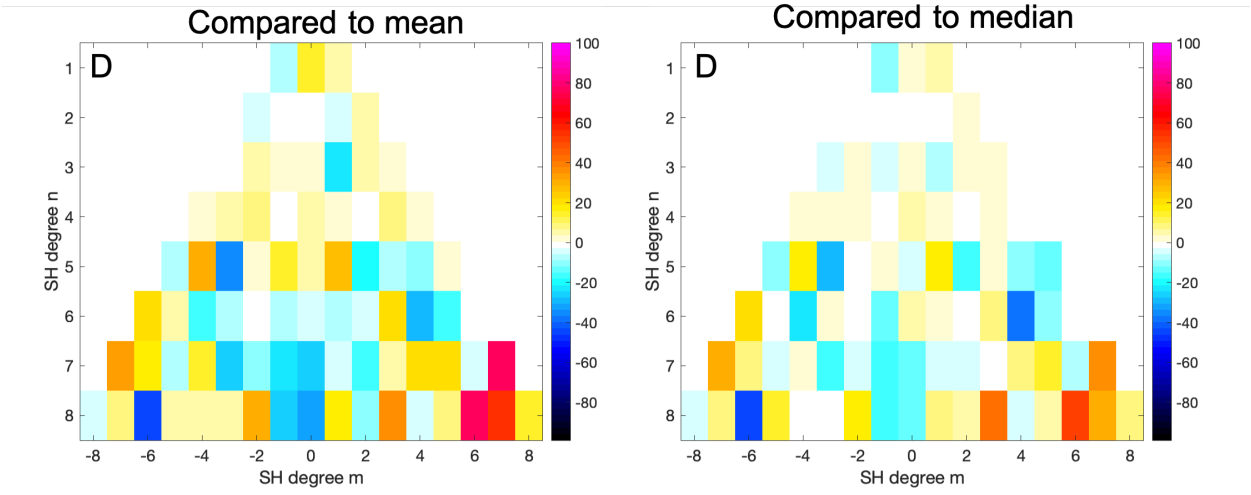

Figure 6: The sensitivity matrices between the D model and the mean (left) and median (right) secular variation models.

7 Residual Analysis

7.1 Swarm - DGRF2015

To evaluate the DGRF 2015 candidate models, we selected Swarm data for a two month period between December 1, 2014 and January 30, 2015. The idea is to compare this short time period of Swarm data with the DGRF candidate models, assuming that the field won't change too much due to SV. The data were downsampled to 1 sample every 10 seconds, and selected at mid-latitudes, equatorward of $\pm 55°$ QD latitude, with local times between midnight and 5AM. We additionally selected quiet data with $Kp < 2$ and $|dRC/dt| <= 3$ nT/hour. The MF7 crustal model and the CHAOS-6 magnetospheric model were subtracted from the Swarm data. Then, we computed residuals between the Swarm measurements and each DGRF2015 candidate model. The residual statistics are presented in Table 2, and the residuals with respect to Swarm A are shown in Figure 7.1. We find similar statistics for all DGRF candidate models, with the exception of model G, which has a significantly higher σ in the Z component for both Swarm A and B. Model H also exhibits an oscillatory trend in its Z residuals which don't appear in other candidate models.

We further investigated the larger Z residuals of the G model by plotting them on a spatial map for Swarm B. Candidates D and H are also shown for comparison. We find significantly larger residuals for model G in the South Atlantic anomaly region, compared with D and H. The oscillatory features seen in the Z residuals of candidate H do not appear to be significant in the spatial map representation.

The median model is closer to both Swarm satellites than the mean model for this two month period centered on 2015.0. This can be seen in the statistics in Table 2, as well as the spatial maps.

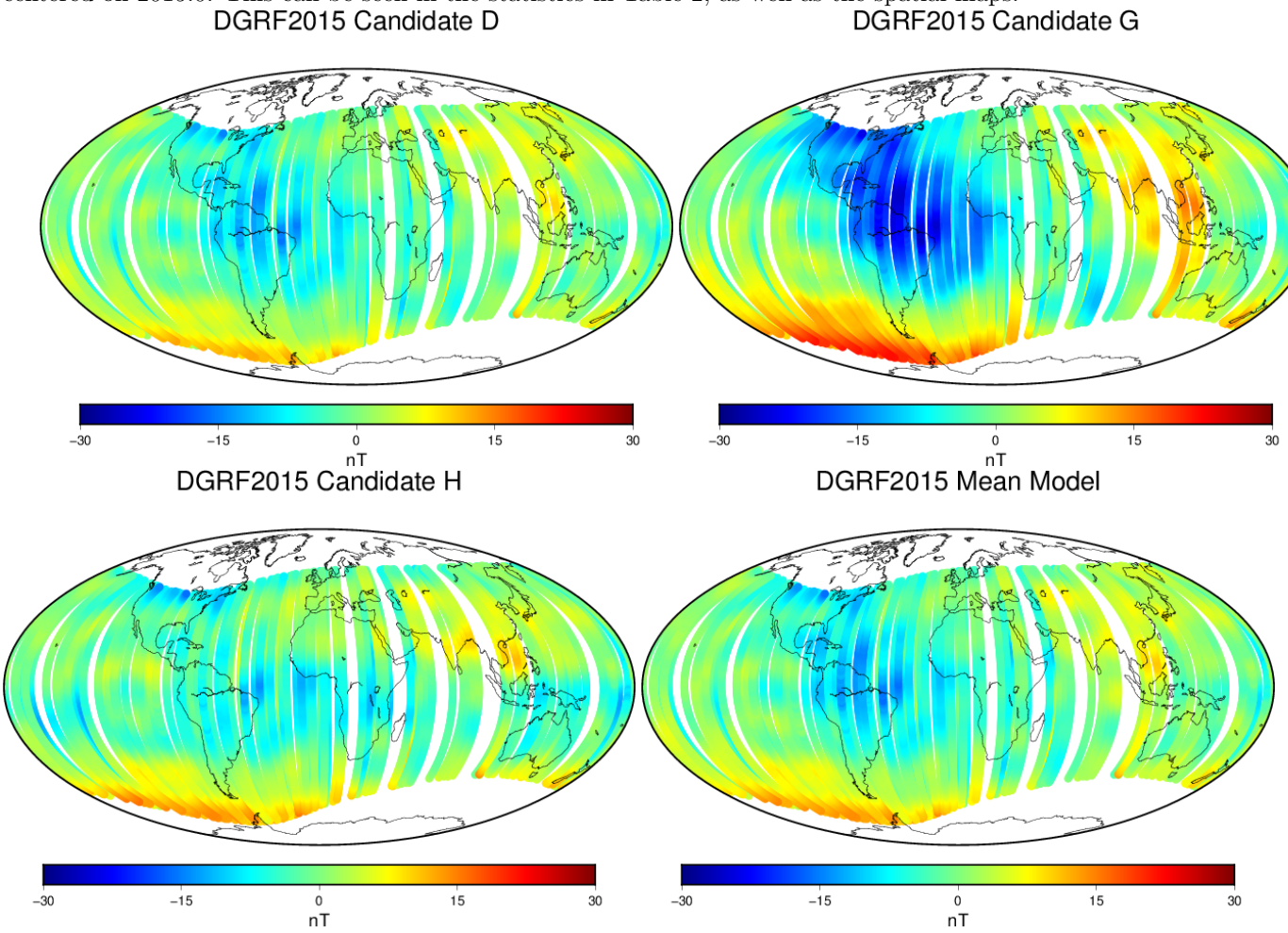

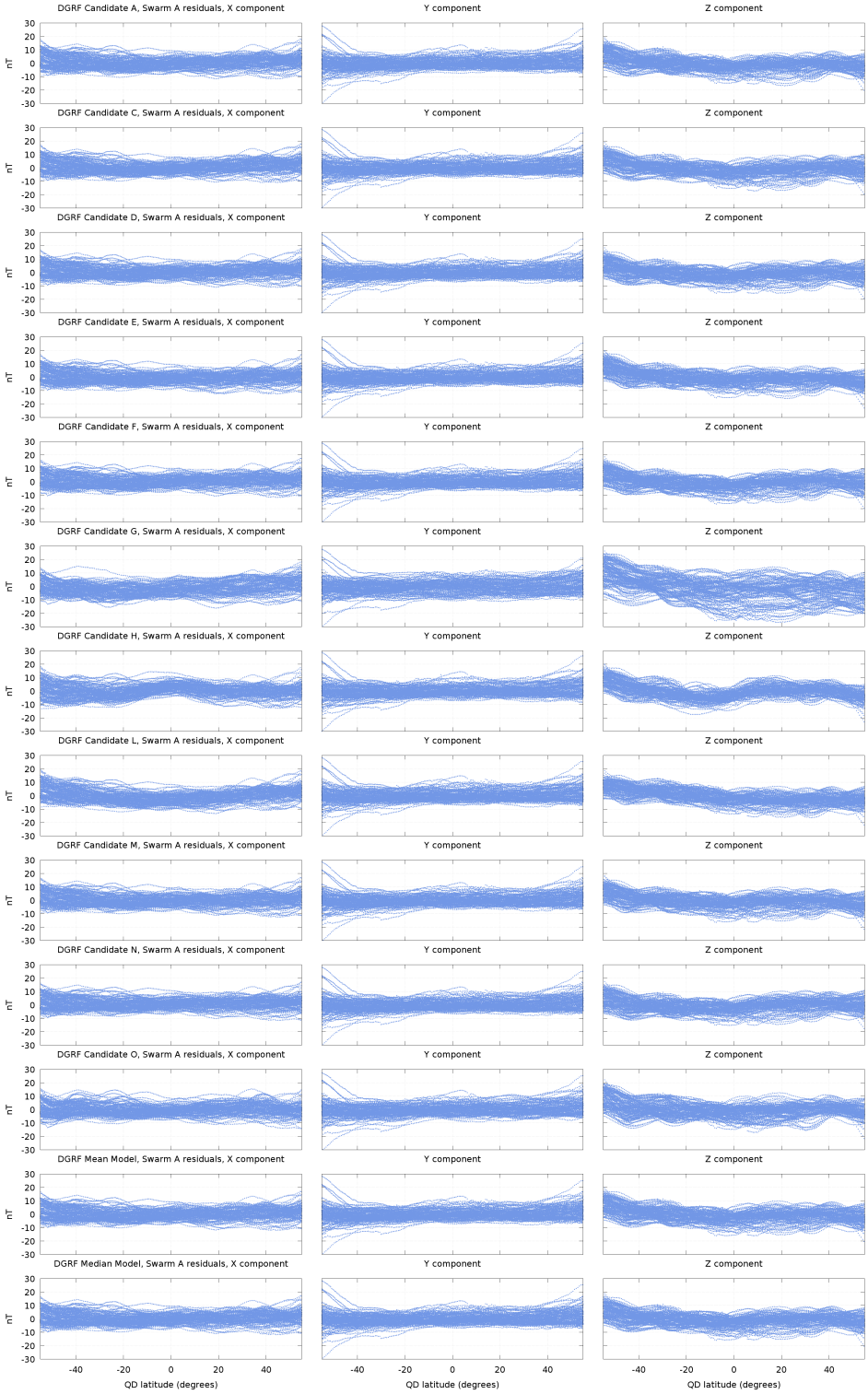
DGRF Candidate A, Swarm A residuals, X component
Y component
Z component
DGRF Candidate C, Swarm A residuals, X component
DGRF Candidate D, Swarm A residuals, X component
DGRF Candidate E, Swarm A residuals, X component
DGRF Candidate F, Swarm A residuals, X component
DGRF Candidate G, Swarm A residuals, X component
DGRF Candidate H, Swarm A residuals, X component
DGRF Candidate L, Swarm A residuals, X component
DGRF Candidate M, Swarm A residuals, X component
DGRF Candidate N, Swarm A residuals, X component
DGRF Candidate O, Swarm A residuals, X component
DGRF Mean Model, Swarm A residuals, X component
DGRF Median Model, Swarm A residuals, X component
nT
30
20
10
0
-10
-20
-30
-40
-20
0
20
40
QD latitude (degrees)

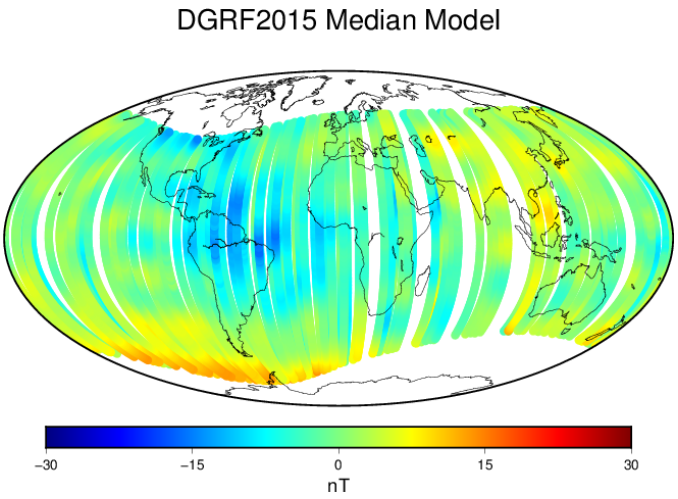
DGRF2015 Median Model
−30
−15
0
15
30
nT

7.2 Swarm IGRF-2020

The IGRF MF 2020 models were compared to Swarm-A measurements between 2019-09-01 and 2019-10-30. To account for the secular variation of the main field between the measurement time and the 2020 model epoch, each MF 2020 candidate model was linearly interpolated using the median DGRF 2015 model. The data selection criteria were similar to those used for the DGRF 2015 comparison to Swarm in section 7.1, with the exception that Dst > -10 nT was used instead of dRC/dt < 3 nT/hr. Also the CHAOS-6 crustal field model was subtracted from the Swarm data rather than the MF7 model. The median interpolated model error relative to SWARM-A has a standard deviation of [4.5 3.2 3.5] nT with the largest errors occurring near 100 deg Longitude. The largest errors are in Candidate E (σ = [5.9 7.9 9.2] nT), and Candidates B, G, H, L and O all have standard deviations of approximately 6 nT. The Bz error has opposite sign near -50 deg Longitude between Candidates G and H, and Candidates B, G, L and O all have similar errors at high latitudes in the southern hemisphere.

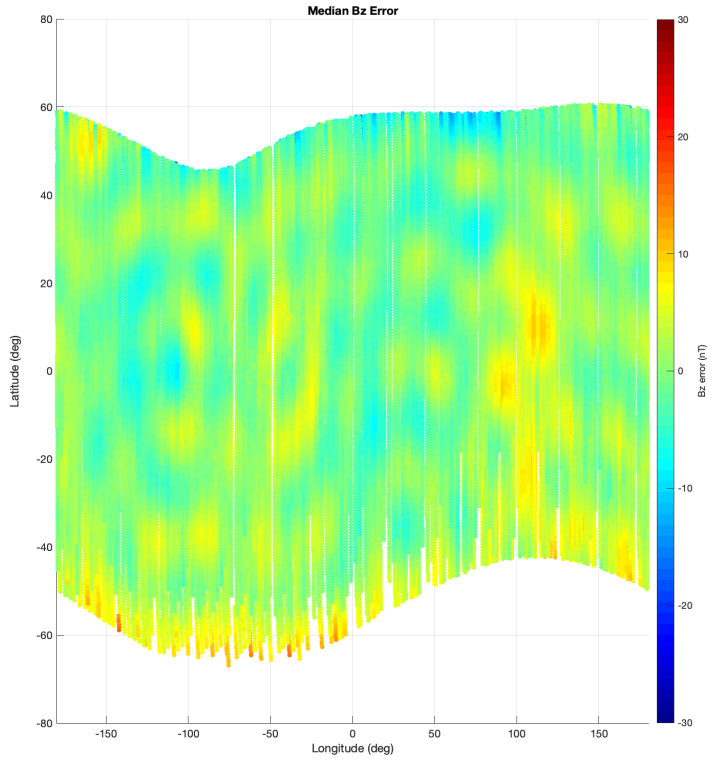

Figure 7: Interpolated Median MF 2020 model Bz residuals relative to Swarm-A

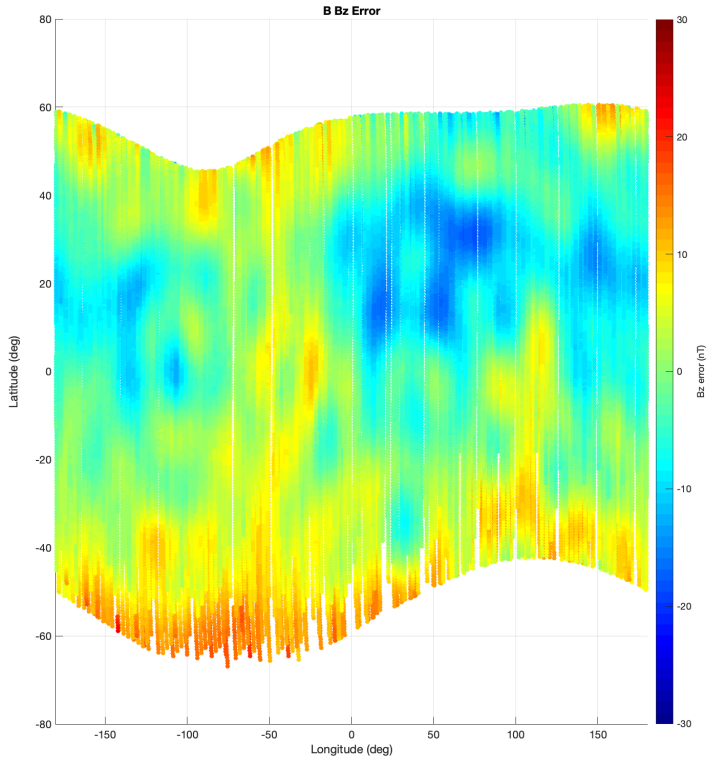

Figure 8: Interpolated Candidate B MF 2020 model Bz residuals relative to Swarm-A

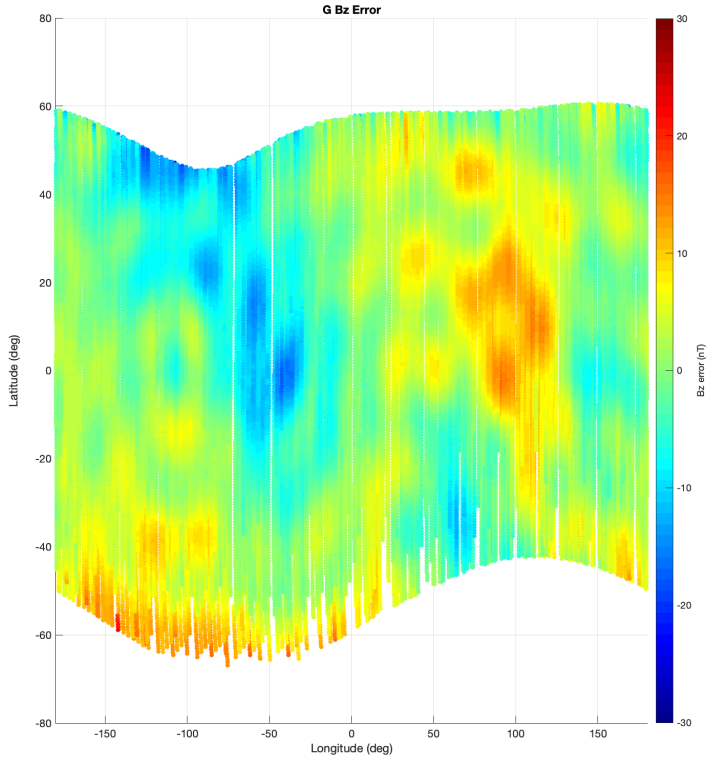

Figure 9: Interpolated Candidate G MF 2020 model Bz residuals relative to Swarm-A

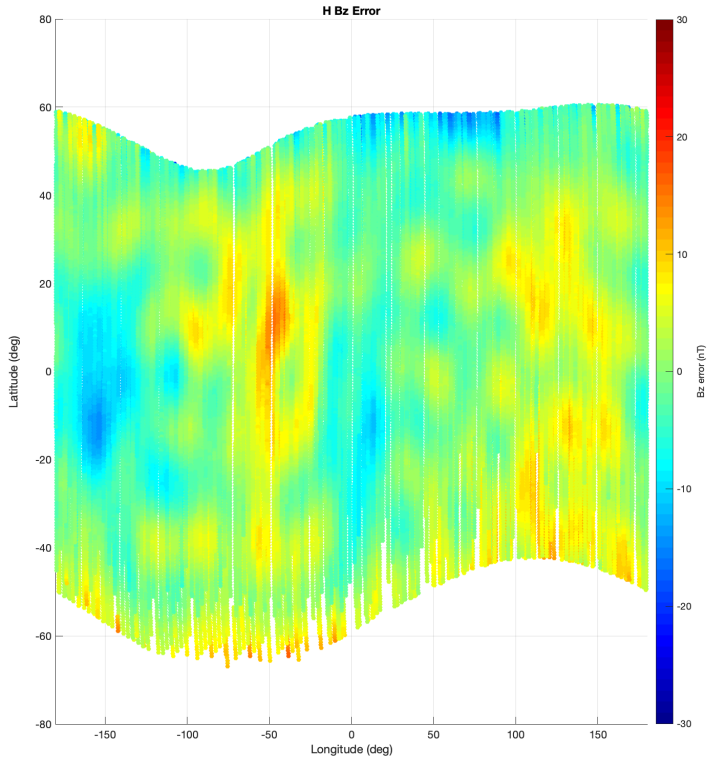

Figure 10: Interpolated Candidate H MF 2020 model Bz residuals relative to Swarm-A

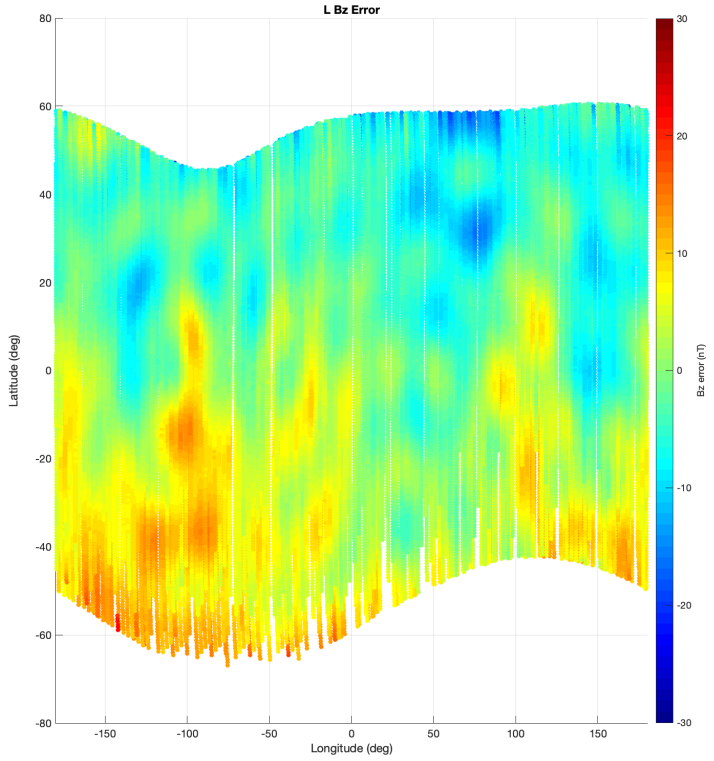

Figure 11: Interpolated Candidate L MF 2020 model Bz residuals relative to Swarm-A

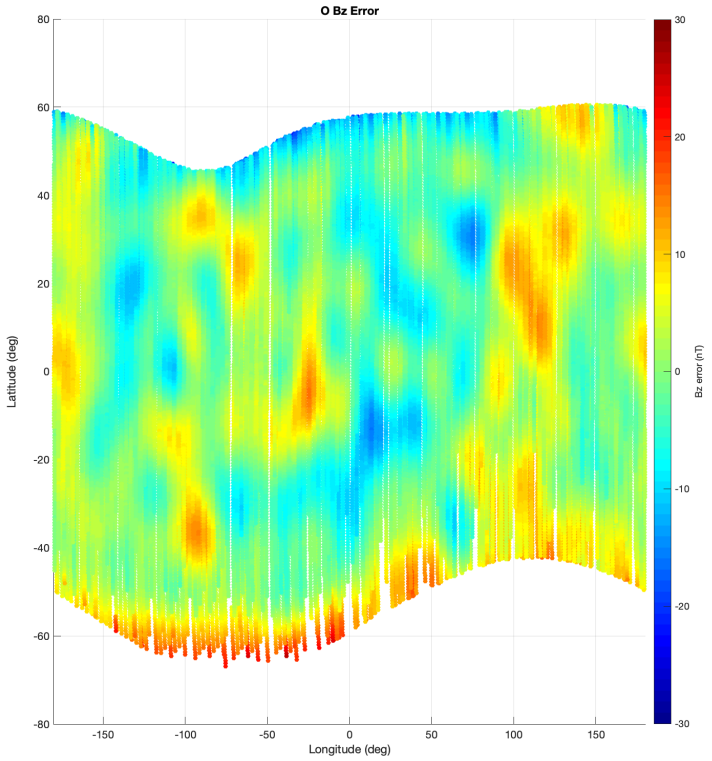

Figure 12: Interpolated Candidate O MF 2020 model Bz residuals relative to Swarm-A

7.3 Observatories

Our aim here is to compare the IGRF-13 candidate secular variation models with a global set of geomagnetic observatory data. We use hourly mean database of geomagnetic observatory data compiled by the British Geological Survey for years 2006-2019 (update of September 2019). We limit the observatories to those located below geomagnetic latitudes of —55—. Observatories with baseline errors, large data gaps were omitted from the analysis. A total of 42 geomagnetic observatories, distributed across the world, were available for the analysis (Figure 13). Most of the observatories have data coverage up to June 15, 2019 (range March 24, 2019 to August 29, 2019). We select data for geomagnetically quiet condition (ap $\leq$ 10) and limit the analysis to 0-5 LT to reduce the influence of disturbance signals. We fit cubic splines with knots separated by 1 year separately to X, Y and Z components in a least-square sense. Secular variation at an observatory was determined by subtracting the spline value at the beginning and end of a year centered on the SV year of the model. The spline model is linearly extrapolated to 2020.0 using the slope at the last knot. We then find the global mean and root-mean-square (RMS) of the differences between model and prediction. Examples of observatory data analysis are shown in Figures 14 to 16.

We find a large variation in the SV predictions of all the candidates as seen in the figures. Table 3 lists the rms differences between the extrapolated observatory splines and candidate models at 2020. Several candidate models have significantly larger rms differences than others. We find the mean and in particular the median model have quite low rms differences compared to the individual candidates.

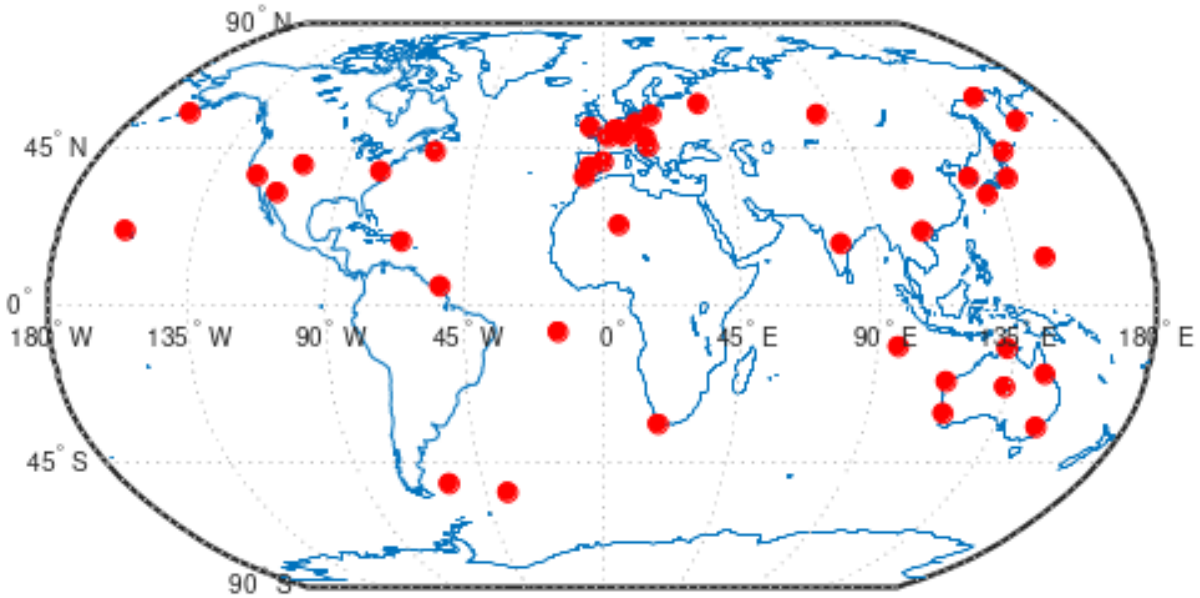

Figure 13: Observatories used for IGRF13 SV analysis

8 Retrospective Analysis of IGRF-12

Our aim here is to compare the IGRF-12 candidate secular variation models (2014 Fall) with a global set of geomagnetic observatory data. We use hourly mean database of geomagnetic observatory data compiled by the British Geological Survey for years 2006-2019 (update of September 2019). We limit the observatories to those located below geomagnetic latitudes of —55—. Observatories with baseline errors, large data gaps were omitted from the analysis. A total of 42 geomagnetic observatories, distributed across the world, were available for the analysis (Figure 1). Most of the observatories have data coverage up to June 15, 2019 (range March 24, 2019 to August 29, 2019). We select data for geomagnetically quiet condition (ap $\leq$ 10) and limit the analysis to 0-5 LT to reduce the influence of disturbance signals. We fit cubic splines with knots separated by 1 year separately to X, Y and Z components in a least-square sense. Secular variation at an observatory was determined by subtracting the spline value at the beginning and end of a year centered on the SV year of the model. The spline model is linearly extrapolated to 2020.0 using the slope at the last knot. We then find the global mean and root-mean-square (RMS) of the differences between model and prediction. Examples of observatory data analysis (Figures 17 to 20).

After the SV residuals were computed for each candidate model against the observatory dataset, we computed rms values of the residuals for the epoch 2017.5. The results are shown in Table 4. We find all candidates have similar rms errors with the truth data, and no model did a particularly better job. This is likely due in part to the geomagnetic jerk which occurred in late 2014. We note that the mean and median models performed slightly better than many of the individual candidates.

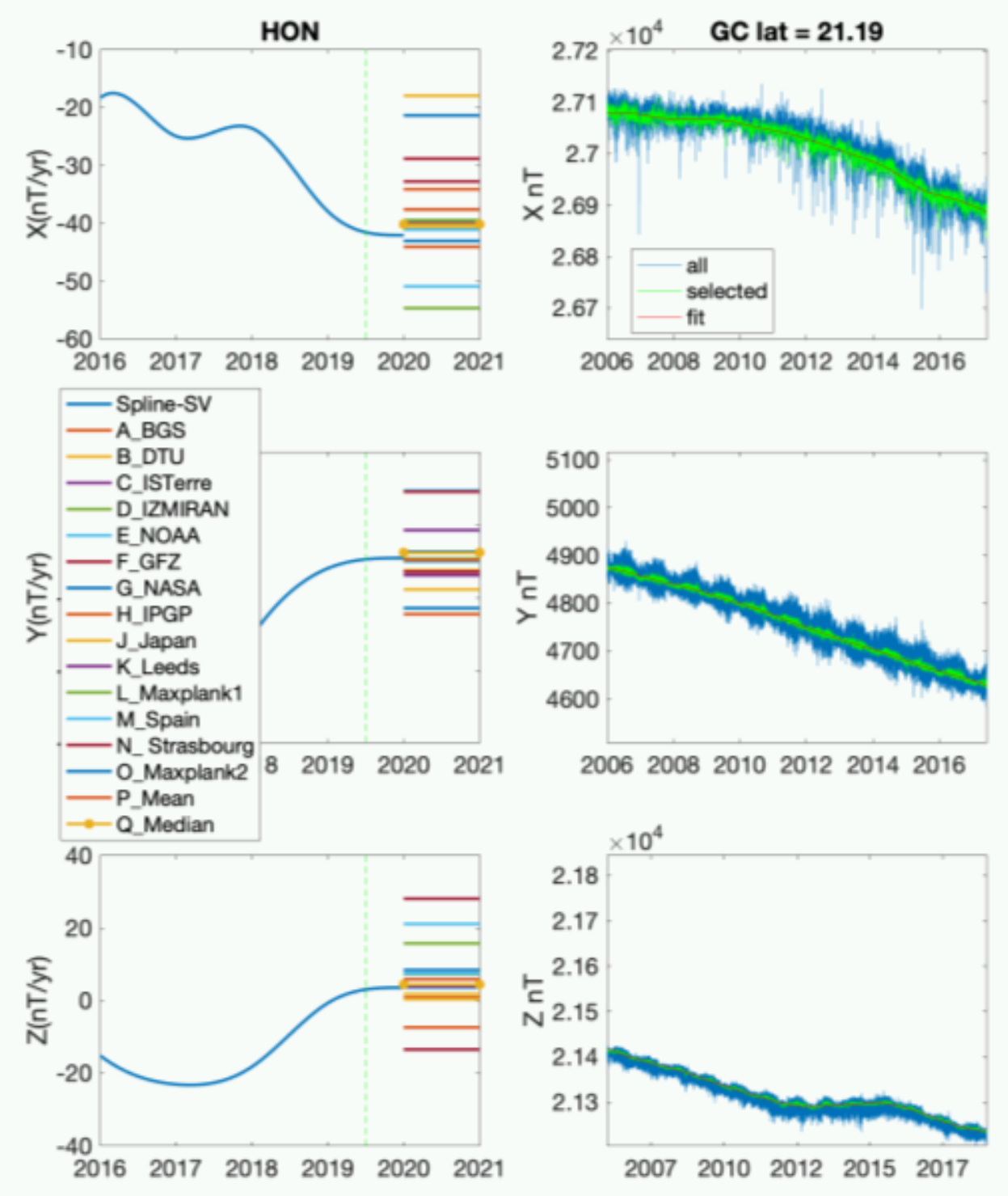

Figure 14: Example of SV determination at station HON. The blue lines on the left panels represent the spline model of the SV obtained from the observatory data. The green vertial lines are the last annual knot (last data point) for the observatory. Right panels show the spline fits to the measured data.

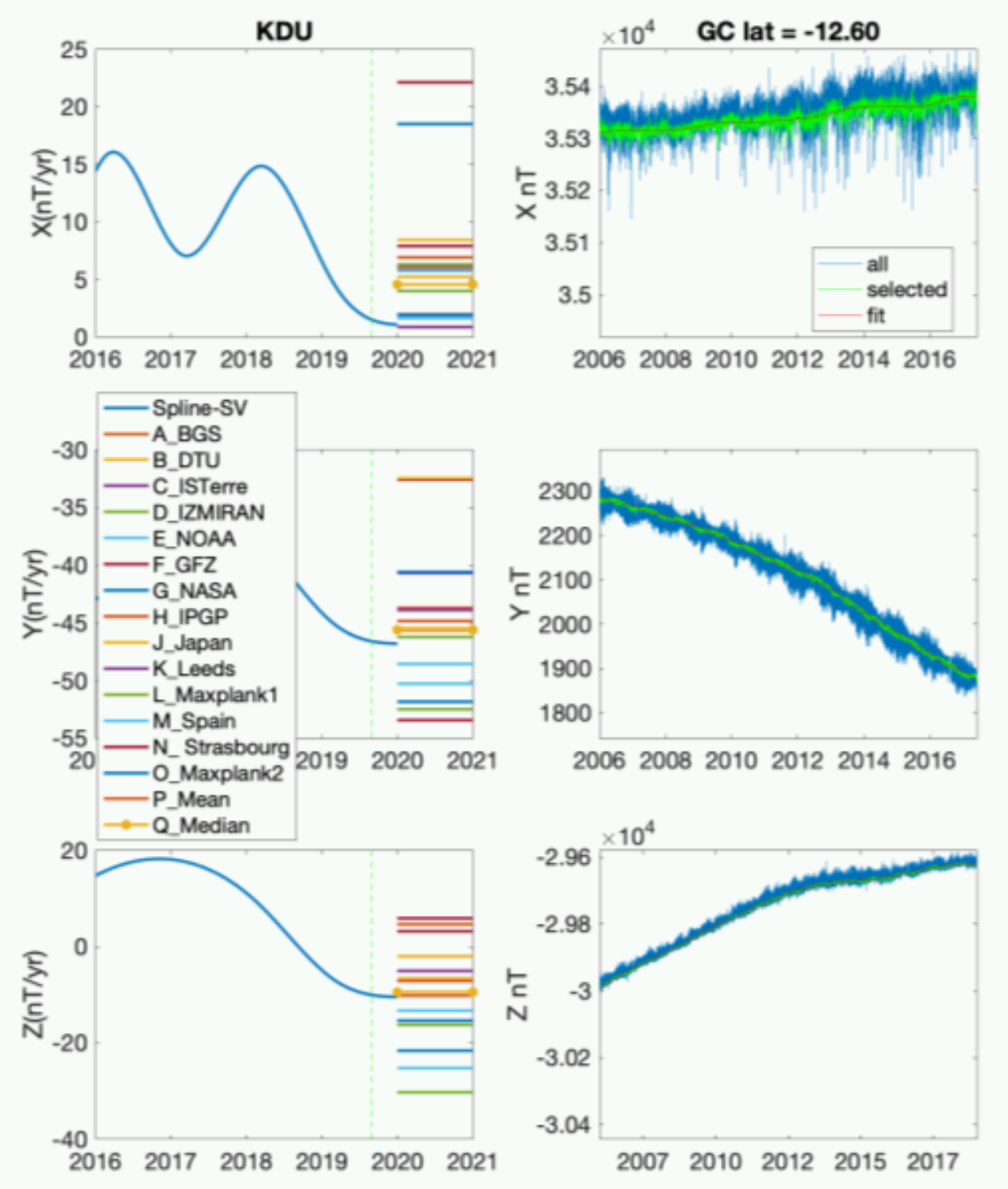

Figure 15: Example of SV determination at station KDU. The blue lines on the left panels represent the spline model of the SV obtained from the observatory data. The green vertial lines are the last annual knot (last data point) for the observatory. Right panels show the spline fits to the measured data.

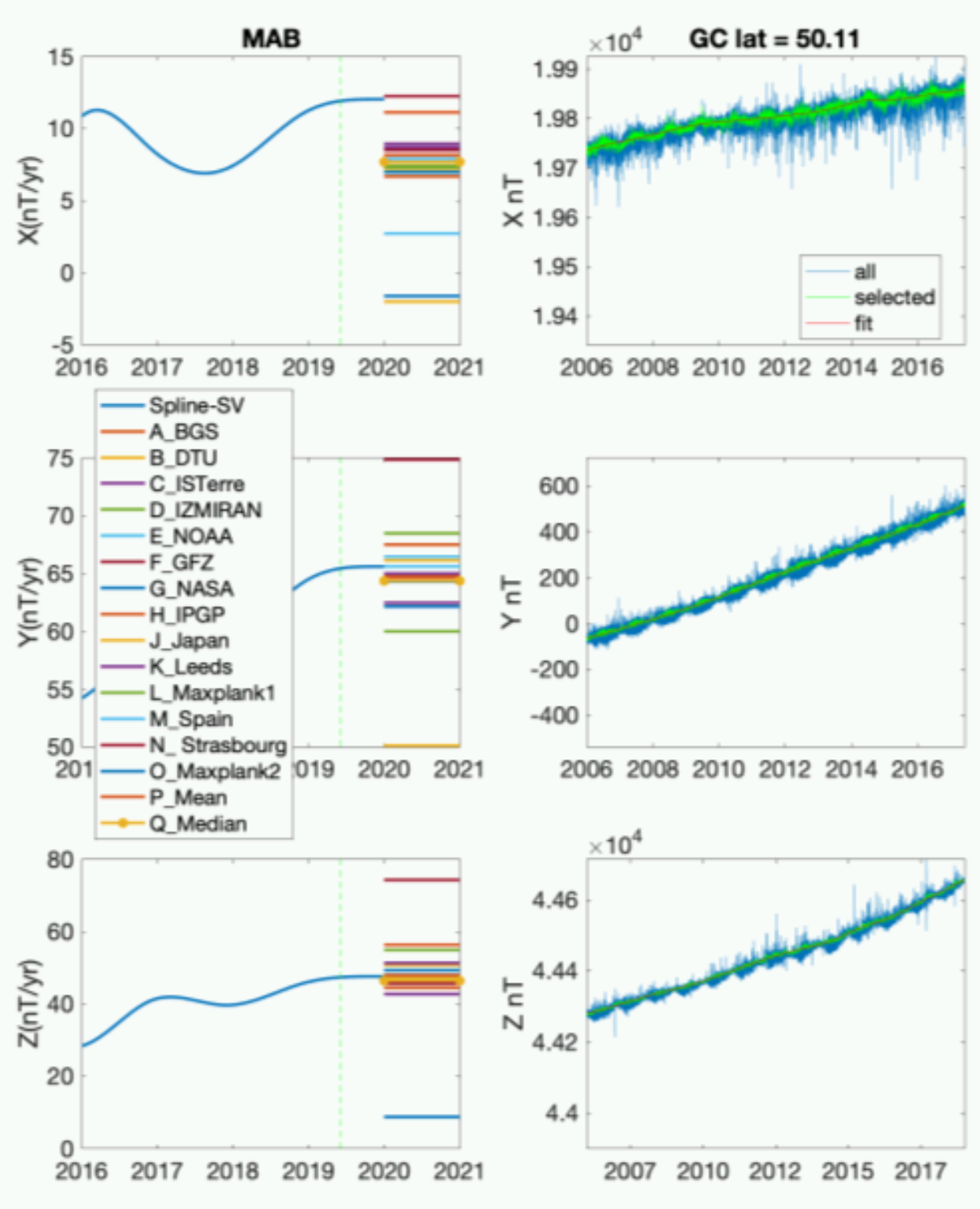

Figure 16: Example of SV determination at station MAB. The blue lines on the left panels represent the spline model of the SV obtained from the observatory data. The green vertial lines are the last annual knot (last data point) for the observatory. Right panels show the spline fits to the measured data.

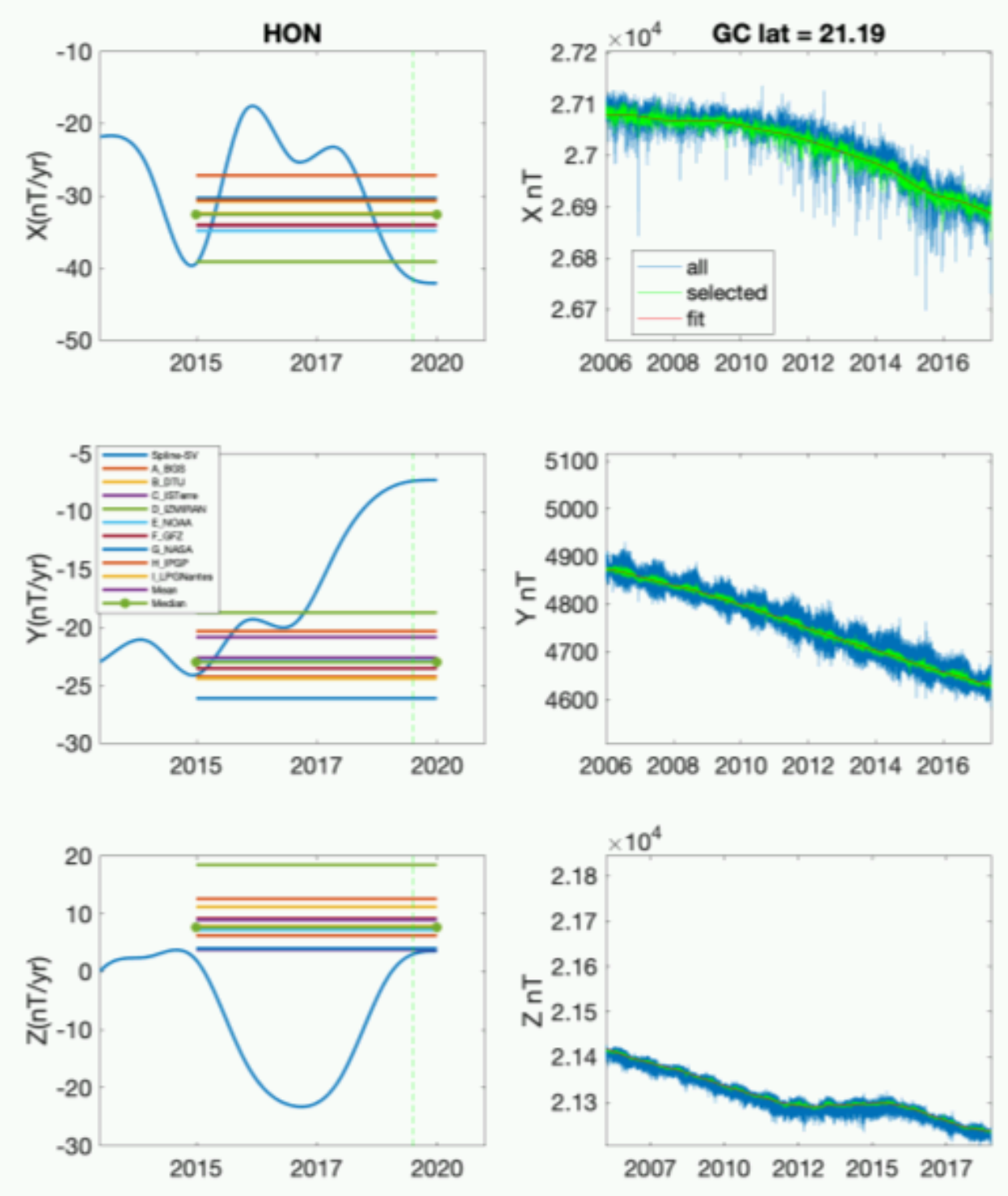

Figure 17: Example of SV determination at station HON. The blue lines on the left panels represent the spline model of the SV obtained from the observatory data. The green vertial lines are the last annual knot (last data point) for the observatory. Right panels show the spline fits to the measured data.

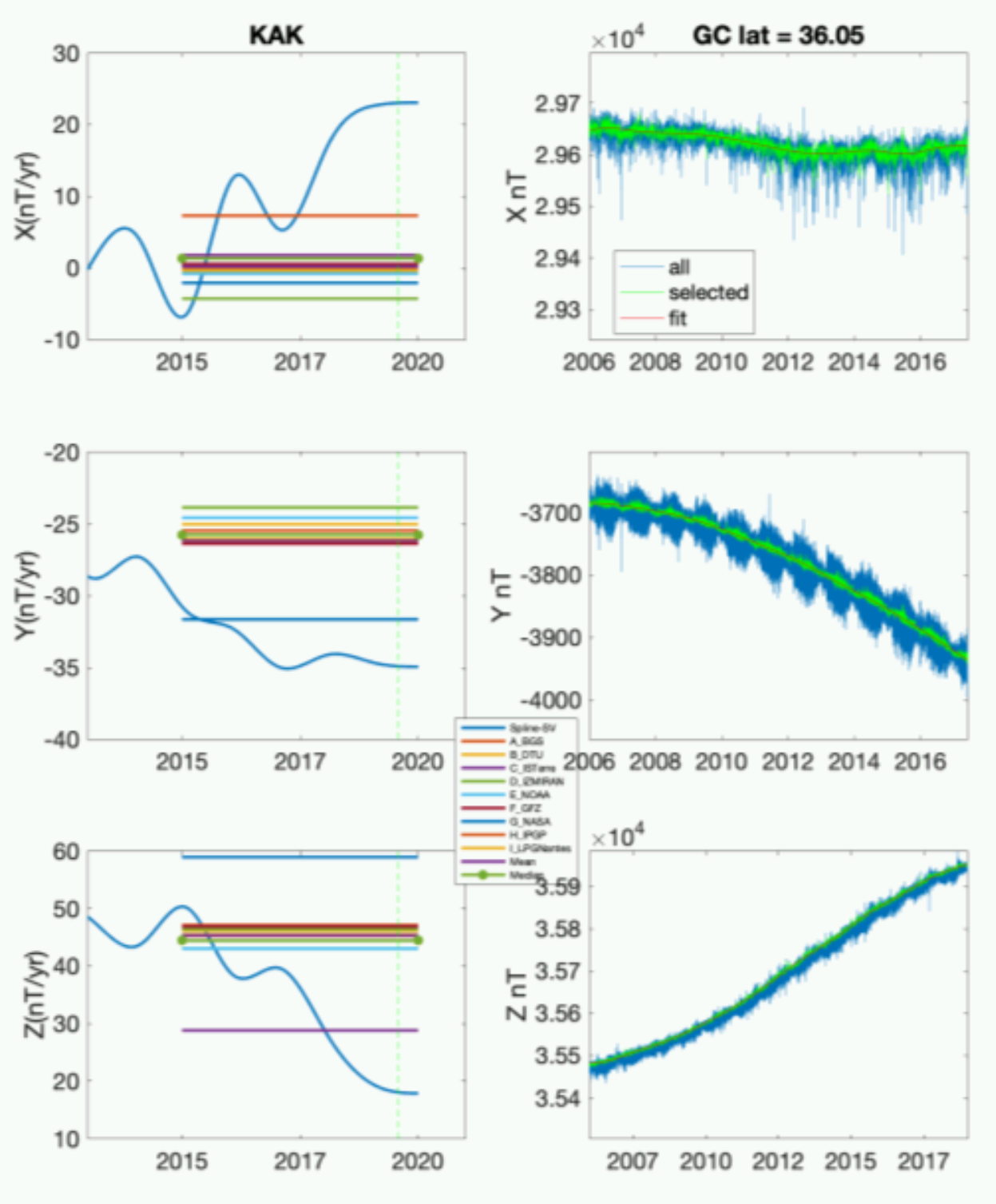

Figure 18: Example of SV determination at station KAK. The blue lines on the left panels represent the spline model of the SV obtained from the observatory data. The green vertial lines are the last annual knot (last data point) for the observatory. Right panels show the spline fits to the measured data.

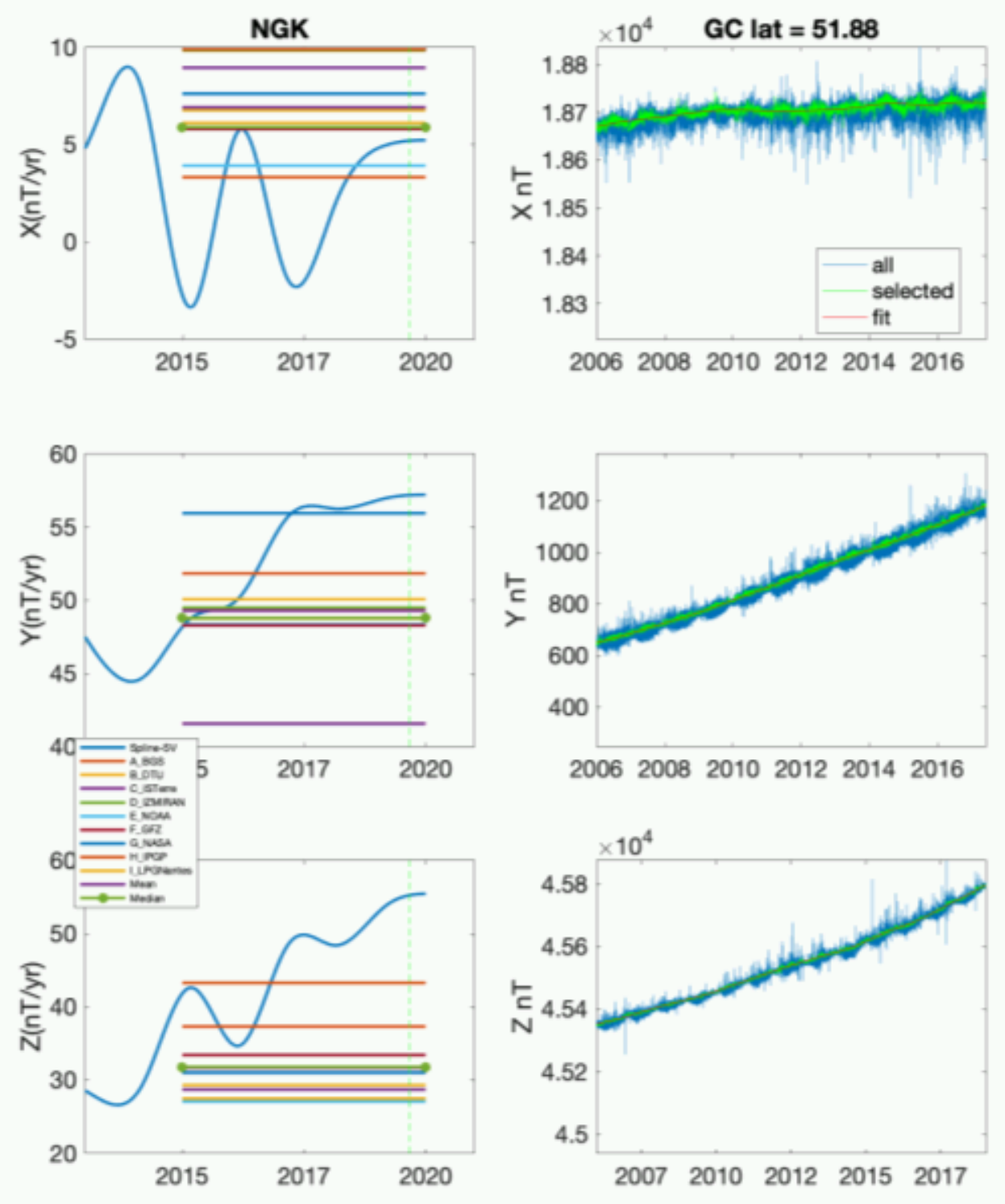

Figure 19: Example of SV determination at station NGK. The blue lines on the left panels represent the spline model of the SV obtained from the observatory data. The green vertial lines are the last annual knot (last data point) for the observatory. Right panels show the spline fits to the measured data.

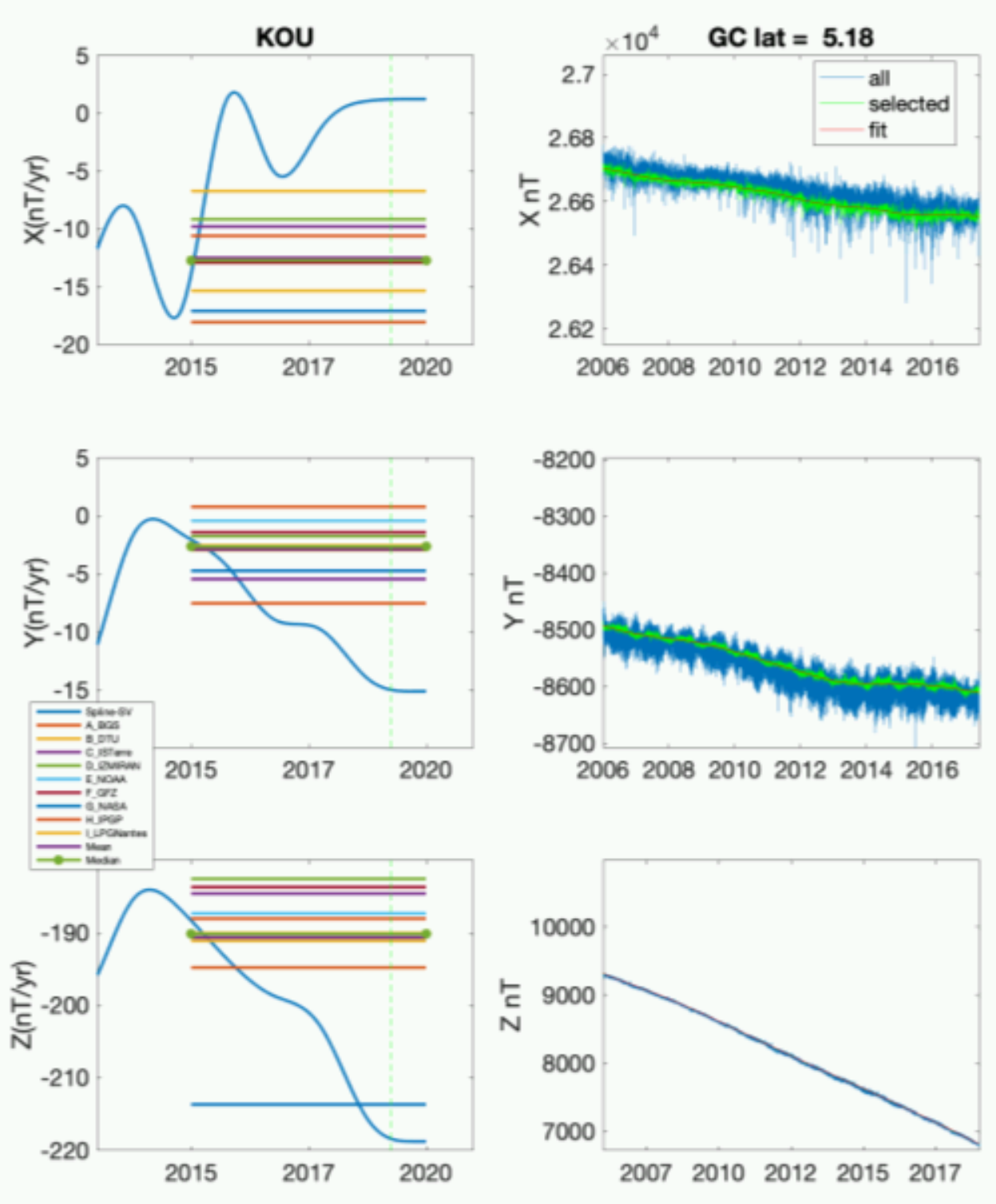

Figure 20: Example of SV determination at station KOU. The blue lines on the left panels represent the spline model of the SV obtained from the observatory data. The green vertial lines are the last annual knot (last data point) for the observatory. Right panels show the spline fits to the measured data.

9 Recommendations

For DGRF2015, we recommend using the **median** model of all candidates. All candidates are quite close to each other, as well as the Swarm data around the 2015 epoch, with the exception of Model G which exhibits a larger difference with Swarm in the Z component. We believe the median model will help to reduce this effect, and we find that the median model is closer to Swarm than the mean model.

For the IGRF 2020 main field model, we recommend using the **median** model of all candidates. This is based on our comparisons with Swarm data in 2019 as well as comparisons betweeen individual candidates and the median model.

For the IGRF 2020-2025 secular variation model, we recommend using the **median** of all candidates. This is for two reasons: (1) there is a large variation among the SV predictions of the different candidate models, with no clear way to determine the quality of any particular model, and (2) our IGRF-12 retrospective analysis found that the median SV model of that epoch performed similarly or better than many of the individual candidates over the 2015-2020 time frame. Our observatory analysis also indicates a few of the candidate models provide outlier predictions at some stations, compared to the rest of the candidates, which is why our preference is to use the median and not the mean. Also, our Table 3 shows that the median model has among the lowest rms differences with our observatory spline analysis at the 2020 epoch, compared with individual candidate models.

Candidate	Swarm A			Swarm B		
	N	mean (nT)	σ (nT)	N	mean (nT)	σ (nT)
A						
X	20,386	0.47	4.22	19,367	0.03	4.47
Y	20,386	0.05	4.16	19,367	2.24	4.20
Z	20,386	-0.50	4.69	19,367	-0.40	4.57
C						
X	20,386	0.59	4.20	19,367	0.14	4.53
Y	20,386	0.05	4.17	19,367	2.25	4.17
Z	20,386	-0.53	4.77	19,367	-0.45	4.74
D						
X	20,386	0.70	4.13	19,367	0.25	4.41
Y	20,386	0.02	4.14	19,367	2.23	4.15
Z	20,386	-0.54	4.59	19,367	-0.44	4.54
E						
X	20,386	-0.24	4.19	19,367	-0.67	4.39
Y	20,386	0.01	4.11	19,367	2.20	4.15
Z	20,386	-0.45	4.80	19,367	-0.37	4.76
F						
X	20,386	0.67	4.10	19,367	0.23	4.41
Y	20,386	0.02	4.15	19,367	2.24	4.15
Z	20,386	-0.56	4.73	19,367	-0.42	4.68
G						
X	20,386	-1.44	4.80	19,367	-1.78	5.27
Y	20,386	-0.30	4.83	19,367	1.98	4.78
Z	20,386	-0.88	8.69	19,367	-0.80	8.34
H						
X	20,386	0.09	4.55	19,367	-0.35	4.80
Y	20,386	0.07	4.18	19,367	2.27	4.24
Z	20,386	-0.40	4.99	19,367	-0.33	4.91
L						
X	20,386	-0.30	4.71	19,367	-0.75	4.84
Y	20,386	0.07	4.21	19,367	2.24	4.20
Z	20,386	-0.45	5.22	19,367	-0.35	5.06
M						
X	20,386	0.17	4.17	19,367	-0.27	4.37
Y	20,386	-0.02	4.14	19,367	2.20	4.16
Z	20,386	-0.53	4.70	19,367	-0.41	4.66
N						
X	20,386	0.98	4.00	19,367	0.51	4.30
Y	20,386	0.00	4.12	19,367	2.22	4.11
Z	20,386	-0.45	4.57	19,367	-0.35	4.58
O						
X	20,386	-0.04	4.24	19,367	-0.47	4.43
Y	20,386	-0.08	4.33	19,367	2.15	4.24
Z	20,386	-0.10	5.25	19,367	-0.06	5.17
Mean Model						
X	20,386	0.15	4.15	19,367	-0.28	4.44
Y	20,386	-0.01	4.14	19,367	2.20	4.15
Z	20,386	-0.49	4.91	19,367	-0.40	4.85
Median Model						
X	20,386	0.44	4.14	19,367	-0.01	4.42
Y	20,386	0.00	4.12	19,367	2.21	4.14
Z	20,386	-0.51	4.66	19,367	-0.41	4.62

Table 2: Residual statistics between DGRF2015 candidates and two months of Swarm A/B data centered on 2015.0

IGRF13 SV Candidate	X (nT/year)	Y (nT/year)	Z (nT/year)
BGS	6.86	4.07	8.08
DTU	5.47	3.51	4.02
ISTerre	5.47	3.51	4.02
IZMIRAN	6.25	4.95	10.41
CU/NCEI	5.50	3.32	9.18
GFZ	7.10	4.83	6.86
NASA	17.78	8.73	27.07
IPGP	5.35	4.86	7.18
Japan	11.92	9.29	12.10
Leeds	5.99	3.68	5.71
MaxPlanck	5.96	4.39	5.44
Spain	5.43	3.46	4.76
Strasbourg	7.89	8.94	17.51
Potsdam	5.82	3.33	5.10
Mean	6.11	3.31	4.52
Median	5.65	3.33	4.02

Table 3: IGRF13 SV candidate model rms differences between (extrapolated) observed and predicted SV at 2020 for the IGRF-13 candidates

IGRF12 SV Candidate	X (nT/year)	Y (nT/year)	Z (nT/year)
A-BGS	8.95	9.13	17.16
B-DTU	9.85	11.67	17.78
C-ISTerre	10.42	13.18	19.47
D-IZMIRAN	10.49	12.63	20.40
E-CU/NCEI	9.61	11.74	18.21
F-GFZ	10.00	11.25	17.10
G-NASA	11.38	10.21	20.91
H-IPGP	9.80	10.77	16.84
I-LPGNantes	9.72	11.60	18.87
Mean	9.64	10.16	17.64
Median	9.43	11.24	17.34

Table 4: IGRF12 SV candidate model rms differences between observed and predicted secular variation at observatories